

PAPER • OPEN ACCESS

Bayesian inference of electron density and ion temperature profiles from neutral beam and halo Balmer- α emission at Wendelstein 7-X







To cite this article: S Bannmann *et al* 2024 *Plasma Phys. Control. Fusion* **66** 065001

View the [article online](#) for updates and enhancements.

You may also like

- [Resonant influence of helicity on Alfvén heating of plasma in stellarators](#)
I O Girka, V I Lapshin and R Schneider
- [Coherence of turbulent structures with varying drive in stellarator edge plasmas](#)
P Huslage, G Birkenmeier, B Shanahan et al.
- [Modeling of the Diffusion of Hydrogen in Porous Graphite](#)
Manoj Warriar, Ralf Schneider, Emppu Salonen et al.

Bayesian inference of electron density and ion temperature profiles from neutral beam and halo Balmer- α emission at Wendelstein 7-X

S Bannmann^{1,*} , O Ford¹, U Hoefel¹, P Zs Poloskei¹ , A Pavone¹ , S Kwak¹ , J Svensson¹, S Lazerson¹ , P McNeely¹, N Rust¹, D Hartmann¹ , E Pasch¹, G Fuchert¹, A Langenberg¹ , N Pablant², K J Brunner¹ , R C Wolf¹  and the W7-X Team³

¹ Max-Planck-Institut für Plasmaphysik, Wendelsteinstr. 1, 17491 Greifswald, Germany

² Princeton Plasma Physics Laboratory, Princeton, NJ 08540, United States of America

E-mail: sebastian.bannmann@ipp.mpg.de

Received 1 December 2023, revised 15 March 2024

Accepted for publication 8 April 2024

Published 18 April 2024



CrossMark

Abstract

By employing Bayesian inference techniques, the full electron density profile from the plasma core to the edge of Wendelstein 7-X (W7-X) is inferred solely from neutral hydrogen beam and halo Balmer- α ($H\alpha$) emission data. The halo is a cloud of neutrals forming in the vicinity of the injected neutral beam due to multiple charge exchange reactions. W7-X is equipped with several neutral hydrogen beam heating sources and an $H\alpha$ spectroscopy system that views these sources from different angles and penetration depths in the plasma. As the beam and halo emission form complex spectra for each spatial point that are non-linearly dependent on the plasma density profile and other parameters, a complete model from the neutral beam injection and halo formation through to the spectroscopic measurements is required. The model is used here to infer electron density profiles for a range of common W7-X plasma scenarios. The inferred profiles show good agreement with profiles determined by the Thomson scattering and interferometry diagnostics across a broad range of absolute densities without any changes to the input or fitting parameters. The time evolution of the density profile in a discharge with continuous core density peaking is successfully reconstructed, demonstrating sufficient spatial resolution to infer strongly shaped profiles. Furthermore, it is shown as a proof of concept that the model is also able to infer the main ion temperature profile using the same data set.

Keywords: electron density profile, beam emission spectroscopy, halo emission, W7X, forward modeling, neutral beam injection, Bayesian inference, Minerva

³ See Pedersen *et al* 2022 (<https://dx.doi.org/10.1088/1741-4326/ac2cf5>) for the W7-X Team author list.

* Author to whom any correspondence should be addressed.



Original Content from this work may be used under the terms of the [Creative Commons Attribution 4.0 licence](https://creativecommons.org/licenses/by/4.0/). Any further distribution of this work must maintain attribution to the author(s) and the title of the work, journal citation and DOI.

1. Introduction

Wendelstein 7-X (W7-X), a magnetic confinement fusion experiment of the stellarator type [1, 2], was successfully optimized for reduced neoclassical energy transport [3]. As many W7-X plasmas are now dominated by turbulent transport the analysis of such is critical to understand high performance discharges and validate predictive models. Density and temperature profiles across the flux surfaces for both electrons and ions are the basis of any particle and heat transport analysis. In dynamic situations, not only the radial gradients but also the time derivatives of the profiles play a crucial role in the analysis, i.e. a profile diagnostic needs to capture both reliably. Thomson scattering, which relies on laser beam scattering on electrons, is the only diagnostic to measure the full electron density profile including the plasma core at W7-X [4, 5]. The absolute density calibration is obtained using the line integrated density measurement of the interferometry system [6]. Due to the importance of plasma profiles in almost all detailed physics analysis it is worthwhile to investigate alternative diagnostic options. The presented technique can be used to cross check and supplement Thomson scattering density profiles. As it is entirely independent of the interferometry system it can offer a valuable validation of electron density profiles at W7-X.

Hydrogen injection in form of a neutral beam (NBI) into a fusion plasma not only serves as a particle and heat source but also enables active plasma diagnostics [7]. The Balmer- α light emitted by excited neutral beam particles and subsequent generations of thermal charge-exchange (CX) neutrals, so-called halo neutrals, contain a rich collection of information on local plasma parameters and beam parameters. In detail, the data contains information on the ion temperature profile, electron density profile, the injected beam power, the beam energy component composition and the alignment of the beam and optical head systems. The local beam emission intensity I_B and halo emission intensity I_H at a point \vec{x} in the plasma reads

$$I_B = n_B^{(3)}(\vec{x}) A_{3 \rightarrow 2} \quad (1)$$

$$I_H = n_H^{(3)}(\vec{x}) A_{3 \rightarrow 2} \quad (2)$$

where $n_B^{(3)}$ is the density of beam neutrals in the $n = 3$ excited energy state, $n_H^{(3)}$ the density of halo neutrals in the $n = 3$ state and $A_{3 \rightarrow 2}$ is the Einstein coefficient of the Balmer- α line. The beam and halo density in any excited state, and thereby also the emission intensity, are linearly proportional to the NBI power. The information on plasma density is contained in both the halo and the beam emission, in two ways. Firstly, the fraction of beam and halo particles in the $n = 3$ state at a certain point in the plasma is determined by a balance of collisional excitation processes and radiative de-excitation processes. The collision rates (electron impact, ion impact, CX) are dependent on the surrounding plasma density. Secondly, the attenuation of the neutral beam particle flux up to the measurement point is determined by ionizing collisions, where, again, the rates depend on the plasma density

along the beam path. Additionally, the spatial extent of the CX diffusion, determining the shape of the halo particle cloud, too, is dependent on the plasma density profile. With such a strong dependence of the emission spectra on the plasma density, it may be possible to infer plasma density profiles from the Balmer- α data alone. To access the information on plasma density a full collisional-radiative (ColRad) model of the beam attenuation and the halo formation is needed. The beam and halo model used for the following analysis is described in detail in [8].

Experimentally, the measured H α -spectrum consists of several components. There are three thermally Doppler broadened components, centered around the H α wavelength of 656.28 nm. The so-called cold H α emission with a very low temperature originating from neutral hydrogen close to the divertor or wall, the passive emission from recycling CX neutrals dominantly from the plasma edge and lastly the emission from the CX halo particles. The light emitted by the beam particles is Doppler shifted depending on the angle between the line of sight and the beam velocity vector. Due to the three distinct neutral beam injection energies and the motional Stark effect (MSE) [9] splitting, the beam emission part of the spectrum is a complex sum of many subcomponents at slightly shifted wavelengths. The H α -emission of neutralized fast-ions is underlying the spectrum but is much weaker than the beam or halo emission. It is not considered and modeled in this analysis. At a wavelength of around 658 nm two carbon emission lines are seen in the spectra.

The main goal of this paper is to study to which extent electron density and ion temperature profiles can be fitted from spectroscopic beam and halo Balmer- α emission data. This is done here using the Minerva Bayesian inference framework [10]. Beam emission spectroscopy using differing elements is a commonly used diagnostic at several fusion experiments. At JET, a lithium beam diagnostic was used in conjunction with Minerva to infer plasma edge density profiles [11]. To measure edge electron temperature and density profiles the emission of a helium beam was used at TEXTOR [12] and at W7-X [13]. The propagation of uncertainties of the helium atomic rate coefficients on the inferred plasma parameters was studied using the Minerva framework in [14]. Using the Balmer- α line and the electron density profile, the deuteron density profile could be reconstructed at JET [15]. Bayesian inference using the Minerva framework has been used successfully at W7X to infer impurity density profiles and the main ion temperature profile using data from a x-ray imaging crystal spectrometer [16]. Active main ion CX spectroscopy was used at DIII-D to measure the deuterium temperature from D α emission [17]. At ASDEX Upgrade a tomographic inversion of five D α spectra was used to measure the ion velocity distribution function in the plasma center [18]. By taking moments of it the parallel and perpendicular deuterium temperatures in non Maxwellian plasmas could be determined.

In section 2 of this paper the detailed and W7-X specific experimental and modeling setup is explained. In section 3 the results of the electron density and ion temperature profile inference are shown and interpreted.

2. Experimental and modeling setup

The NBI system at W7X was built to operate up to eight individual sources injecting neutral hydrogen, deuterium or helium into the plasma with an accelerating voltage of up to 55 keV. In the 2018 operational phase ('OP1.2b'), on which the analysis focuses in this paper, sources S7 and S8 were operated [19, 20].

The spectroscopic system measuring the active hydrogen Balmer- α emission consists of up to 54 lines of sight viewing the neutral beams S5, S6, S7, S8 from three different ports (AEA21, AEM21, AET21), i.e. from three different viewing angles. In this analysis only data from the AEM21 and AEA21 port are used. The line of sight intersections with the beam axes are evenly spaced (≈ 5 cm) along the axes. The system is described in detail in [21]. Each line of sight is absolutely intensity calibrated. An overview of the neutral beam injection and beam emission spectroscopy geometry is shown in figure 1. In the left plot a slice in the Rz -plane along the beam axis of source 8 is plotted. The modeled neutral beam density is shown in a red color scale and the flux surfaces are drawn as blue contour lines. The beam emission measuring locations of the A port lines of sight are shown as blue dots and follow the neutral beam axis from the low field side plasma edge to mid plasma radius on the high field side. The M port lines of sight are shown as green dots and cover a slightly smaller range along the beam. A top down view and a beam cross section view of the line of sight geometry viewing the neutral beams is shown on the right side of figure 1.

A forward model computing the beam attenuation and the halo formation was implemented in which each source is described as the sum of several Gaussian pencil (Gausscil) beams. For each Gausscil the attenuation and emission due to the interaction with the plasma is calculated solving a step wise ColRad model along the beam axis. The MSE and the effect of elements in the optical path from the plasma to the spectrometer are included in the spectra prediction. The halo formation and its $H\alpha$ emission are computed by solving a coupled, ColRad CX diffusion equation with the beam-plasma CX reaction rate being the initial source term. A detailed description of the model and its verification can be found in [8]. A simplified graph diagram of the implemented beam and halo emission forward model described in [8] is shown in figure 2. The free parameters which can be inferred by the model from the beam and halo emission data are drawn as blue ellipsoids.

The plasma ion composition enters the model in two places as an over the plasma radius averaged Z_{eff} value. Firstly in the beam attenuation calculation where currently a pure hydrogen plasma is assumed. Secondly in the halo calculation where $Z_{\text{eff}} = 1.2$ is assumed which is a typical value for W7-X plasmas [22]. It was quantitatively shown that varying Z_{eff} in the full range of expected values ($1.0 < Z_{\text{eff}} < 1.5$) in both, the halo and the beam calculation, introduces an uncertainty of the inferred profiles of up to 6%. Since Z_{eff} enters the model, it is theoretically possible to perform inference on this parameter, as explored previously [15]. However, in this case the dependence is too weak to provide a useful constraint on Z_{eff} .

To deal with the complexity of the multivariate dependencies of the measured $H\alpha$ spectra all models are implemented in the Bayesian analysis framework Minerva [10]. The framework allows for a consistent set up of the models in a Bayesian network structure and facilitates the inference process of any declared free parameter while including the data of all available lines of sight. The free parameters of the model can be divided into three groups and are shown in table 1.

The optical head alignment (expressed as rotations: pitch, yaw, roll) determines at which flux surfaces the lines of sight intersect the beam and this is not expected to change significantly over the course of a measurement campaign. Equally, the beam divergence and the beam alignment are assumed to remain constant. To save computing time, they are only inferred on a small number of discharges, using plasma profiles provided by other diagnostics and then kept constant at these values for the following inference process of profiles on other discharges. The Thomson scattering system [4] combined with interferometry [6] was used to get electron density profiles in these cases and the CX recombination system (CXRS) [21] measuring carbon impurity radiation was used to get ion temperature profiles. It was assumed that the main ions (protons) have the same temperature as the impurities. The Balmer- α emission of beam and halo is only weakly dependent on the electron temperature profile. Therefore, the profile can not be inferred by the model but is set using the Thomson scattering diagnostic data.

To give an impression of the used data and the fit quality of the model, the measured and fitted spectra of four example lines of sight are shown in figure 3. The free parameters in the fitting process were the electron density profile and the total beam power. The lines of sight plotted on the left (right) side are both viewing the beam close to the plasma edge (core) but from different angles, which leads to an opposite Doppler shift of the beam emission spectroscopy (BES) components (shown as filled, gray graph). Due to the viewing geometry on the beam and the magnetic surfaces the lines of sight with a horizontal view have a better radial resolution in terms of the effective radius r_{eff} . At a wavelength slightly higher than the Balmer- α line there is a carbon impurity line which is estimated from the spectra before the NBI is active. The thermally Doppler broadened emission of the halo particles is shown in orange. As the halo particles are at a higher temperature than the recycling hydrogen particles, the emission line is broadened more strongly. No model of the cold passive $H\alpha$ emission (shown in blue) is implemented and this peak is freely fitted for each channel at a time point before the NBI was activated and is assumed to be constant over the course of the discharge. In purely NBI heated discharges this assumption of a constant passive signal over the course of a few seconds becomes questionable as the additional NBI power and fueling influences the hydrogen recycling in the machine. In these cases the wavelength intervals containing the cold $H\alpha$ and carbon emission are excluded entirely during the inversion making a fit of the passive signal obsolete. The information of the BES emission which is Doppler shifted into these excluded ranges is then lost. The level of Bremsstrahlung is

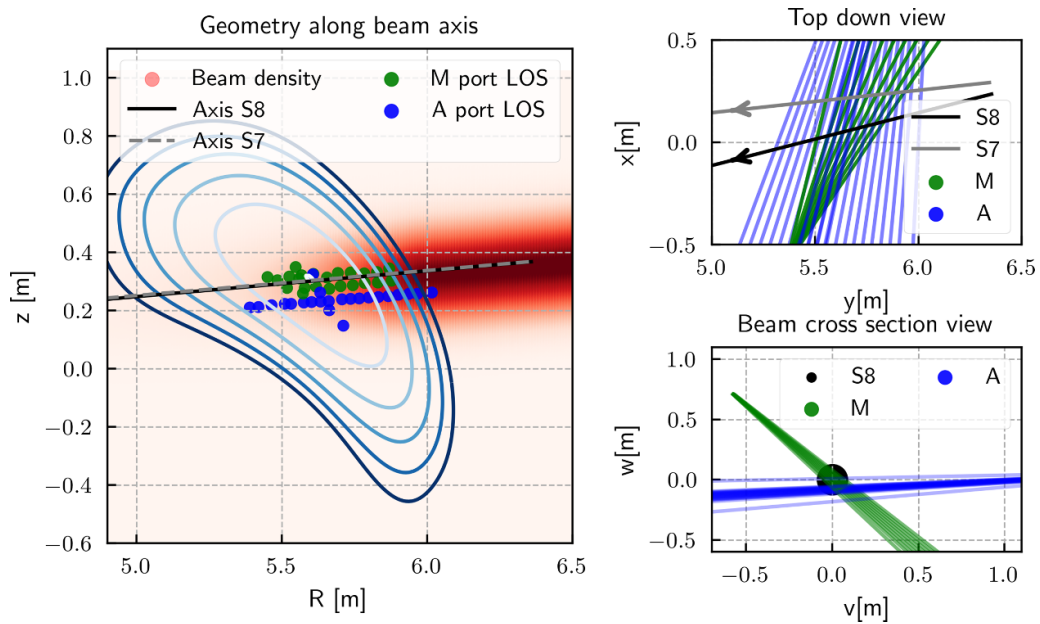


Figure 1. Neutral beam injection and beam emission spectroscopy geometry at W7-X. Left: represents a cut in the Rz -plane along the beam axis of source 8. The modeled neutral beam density is shown in a red color scale, visualizing the beam attenuation on its way through the plasma. The flux surfaces are drawn as a contour plot with blue colors. The beam emission measuring locations of the lines of sight of AEA21 (A) and AEM21 (M) port are shown as blue and green dots. Right: top down and beam cross section view of the lines of sight geometry on the neutral beams S7 and S8. The A port lines of sight have a nearly horizontal view on the beam while the M port lines of sight have a more tilted view from above the beams.

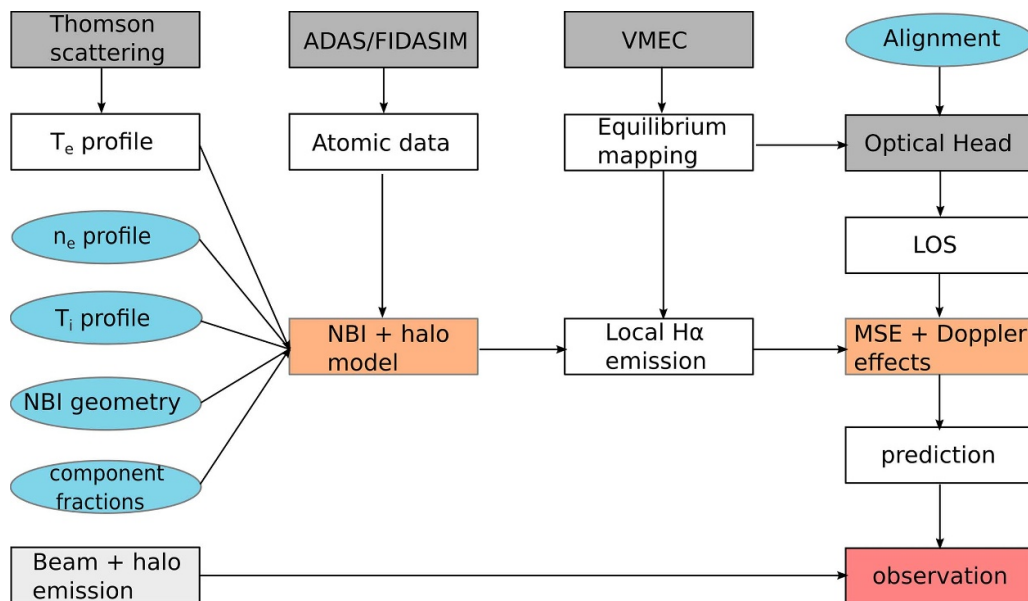


Figure 2. A simplified graph diagram of the beam and halo emission forward model implemented in the Bayesian analysis framework Minerva. The input parameters which can be inferred from the data are shown in blue.

estimated in each spectrum from the data at the edges of the measured wavelength interval as there is no beam or halo emission present. It can be seen that it is significantly smaller than the measured $H\alpha$ emission.

The free parameters are inferred from data of 54 lines of sight using the maximum *a-posteriori* (MAP) estimator of the Minerva framework which yields the most probable state of the model parameters to explain the measured data.

In Bayesian statistics the MAP result can be seen as the equivalent to the maximum-likelihood estimate. Detailed equations can be found e.g. in [11]. The statistical error on the fitted parameters introduced by statistical uncertainties of the data and the model input parameters (represented as prior probability distributions in the Bayesian model) is computed using the Laplace approximation. Systematic errors in the data and the used forward model are not straightforward to take into

Table 1. Parameters of beam and halo forward model. Bold parameters are used as free parameters in the following analysis. The other parameters are inferred on other discharges and then held fixed at the stated values. As data is used from two optical heads (called A and M [21]) there are two values given. The beam component fractions p_i describe the fraction of beam power injected with a particle energy of $\frac{E_i}{E}$.

Beam	Optical head (A/M)	Plasma profiles
Power	Pitch = (0.5°/−1.1°)	Electron density
Divergence = 0.75°	Yaw = (−0.1°/−1.9°)	Ion temperature
Alignment: 5 cm beam upward shift	Roll = (0.°/0.°)	Electron temperature
Component fractions (p_1, p_2, p_3)		

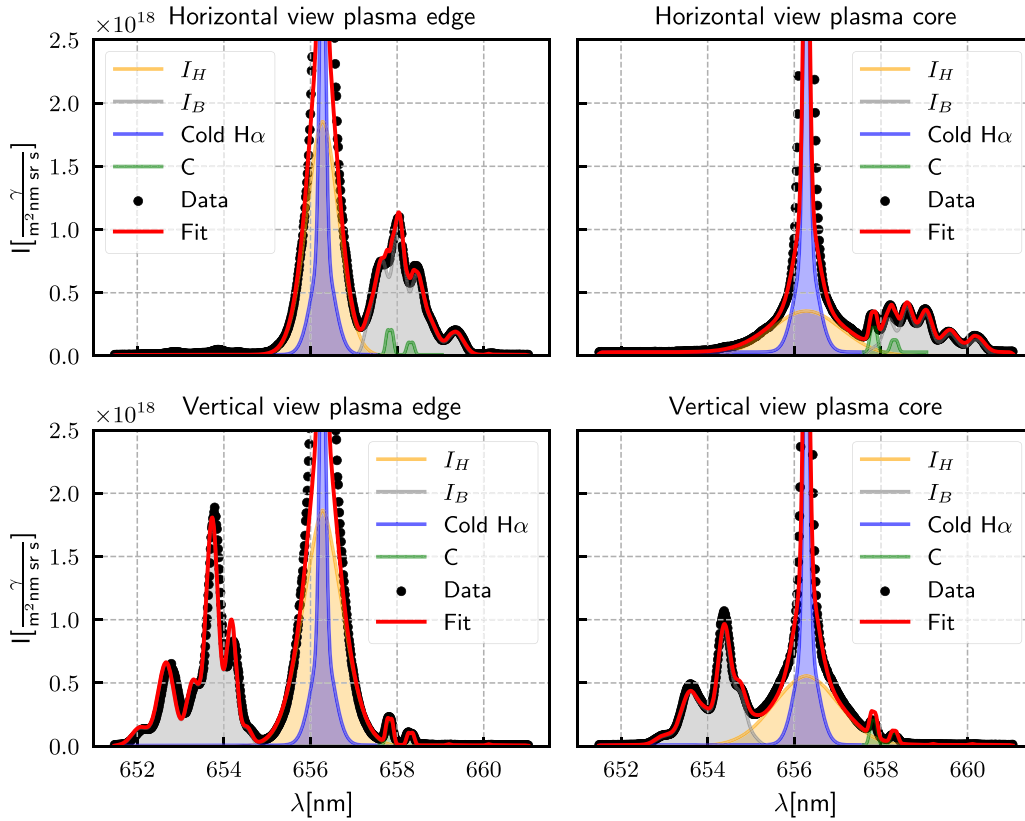


Figure 3. Comparison of measured (black dots) and fitted (red line) full Balmer- α emission spectra for 4 different lines of sight in a discharge with a single active NBI source (#20180920.017). The fitted spectra are composed of the beam emission (gray), halo emission (orange), cold H α emission (blue) and two carbon impurity lines (green). The shown lines of sight intersect the beam at different positions in the plasma and under different viewing angles. Upper (lower) left: horizontal (vertical) view of the beam and the active signal comes from the plasma edge. Upper (lower) right: horizontal (vertical) view and the active signal comes from the plasma core.

account as the sources are not known. To get an estimate of the systematic uncertainty of the fitted plasma profiles seven individual profiles are inferred for each time point. In four cases exclusive subsets of data are used which all in itself contain the full information on the electron density and ion temperature profile. The subsets are defined by using data solely from either one of the two used optical heads (AEA21-A, AEM21-S7/8) or restricting the used part of the measured spectra to infer exclusively from beam or halo emission data. The other three cases use all data available but Z_{eff} is varied between 1.0 and 1.5. Finally, the standard deviation of the fitted values in all cases is used as the systematic error estimation. It was found that the systematic errors computed in this way strongly dominate by an order of magnitude over any statistical errors computed with the Laplace approximation. The reason

for this finding is the negligible statistical error on the measured Balmer- α data.

3. Results

3.1. Electron density profile inference

The inference of electron density profiles from beam and halo emission data is tested on four different discharges. No fixed model parameters are changed in between and the same set of lines of sights is used. The time points analyzed in three of the discharges (20180920.009/011/017) represent electron cyclotron resonance (ECR) heated plasmas in steady state conditions at different line integrated density levels. To obtain beam emission data, NBI blips of 20 ms are injected into

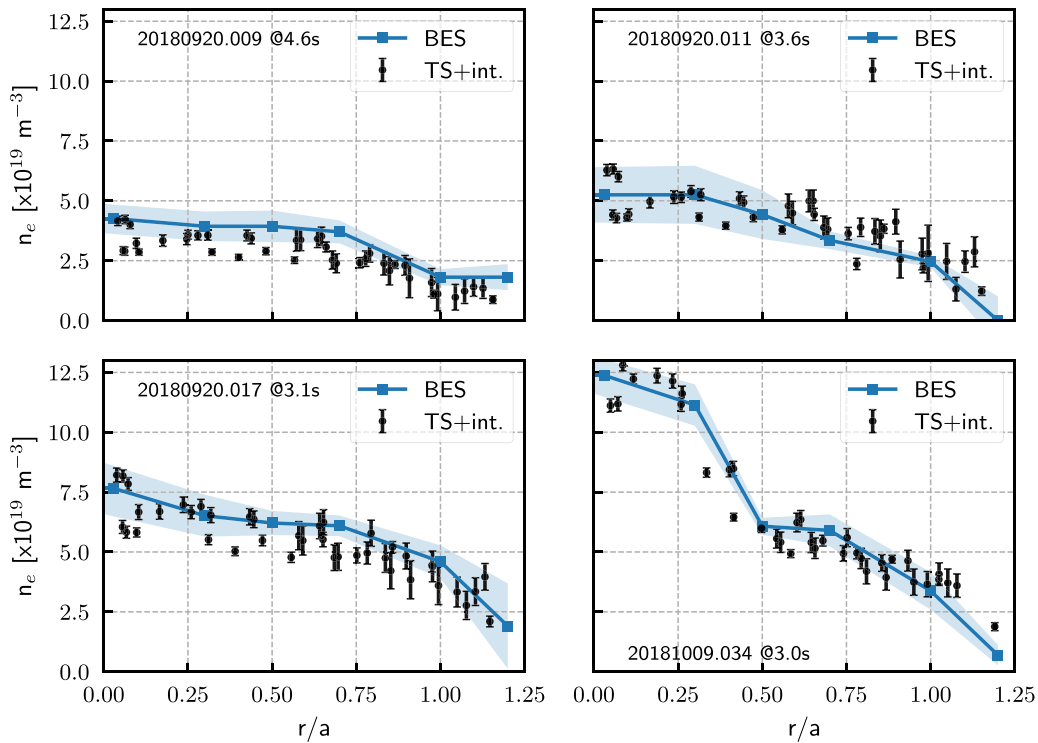


Figure 4. Inference of the electron density profile solely from beam and halo H α emission data. The inferred profiles (blue line + squares) are compared to the raw data points of the Thomson scattering system (black dots) normalized against the line integrated density measured by the interferometer. The squares with the linear interpolation in between represent the parameterization of the density profile in the model. The discharges 20180920.009/011/017 are ECR heated and 20 ms NBI blips were applied. These discharges were in a steady state at the shown time points. The discharge 20181009.034 has a long, purely NBI heated phase and exhibits a peaked density profile which continuously changes over the course of the NBI phase.

the plasma. The time point analyzed in the fourth discharge (20181009.034) lies in a purely NBI heated plasma phase with a continuously peaking, so non steady state, density profile. These shots span almost the complete range of conditions in the experimental campaign, with the exception of very high density O2-ECR heated discharges, where no shots with NBI blips were available.

In figure 4 the results are shown (blue squares + line) and compared to data from the Thomson scattering system (black dots) which are normalized against the line integrated density measurement from the dispersion interferometer system [6]. In the model the electron density profile is represented as a piecewise linear curve with the plotted squares as the free parameters. In all cases, so for flat density profiles at different magnitudes and for the peaked profile, a good agreement is achieved. To get a stable fit, the radial resolution was set to six points over a range from $r/a = 0.0$ to 1.2 . These points can be freely chosen and do not represent the measurement locations which are all simultaneously taken into account. The number of points must be chosen high enough to capture the desired length scales in the profile, but low enough not to introduce too much noise where insufficient information is available in the data. Typically this is significantly lower than the ~ 50 measurement points included in the data. All data was averaged over 20 ms which is the NBI blip time window. In the current state the model is not able to infer the profiles on a

much finer scale than the used coarse grid of six points ranging from $r/a = 0$ to $r/a = 1.2$. It was found that a higher number of points does not increase the inferred information but yields noisy profiles with non-physical gradients. Future work starting from these results could investigate the possibility of Gaussian process fitting of the profiles and training its hyper parameters from the BES data, thereby increasing the number of radial grid points while enforcing a certain profile smoothness. In a physical sensible profile in flux coordinates the radial gradient at $r/a = 0.0$ has to be 0 for it to be continuous. However, there is not enough data to reliably infer the profile gradient around $r/a = 0.0$, i.e. a vanishing gradient at the very core has to be enforced if these profiles are used in further analysis.

In some discharges at W7-X with pure NBI heating phases, a gradual, dynamic peaking of the density profile in the plasma core can be observed. To study the sensitivity of the density profile inference to temporal changes in the plasma core, the discharge 20181009.034 is analyzed at four time points between 1.2 s and 3 s. In this phase of the discharge the NBI is the only heating source and a peaked density profile is measured by the Thomson scattering system.

In the top plot of figure 5, the inferred density profiles are shown and compared to the Thomson scattering data at each time point. The profiles evolve only in the plasma core at radii $r/a < 0.5$ and this evolution is well captured by the

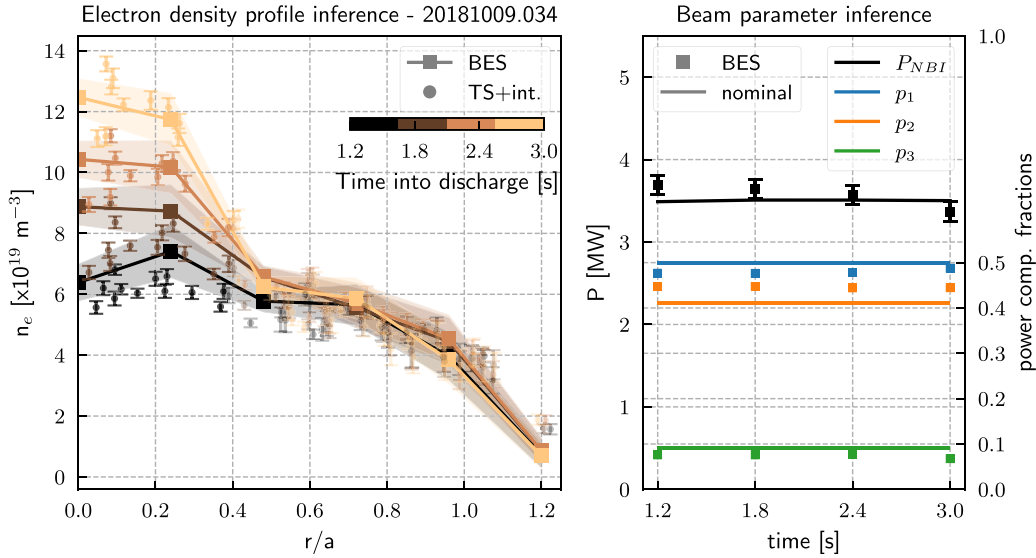


Figure 5. Left: inference of the electron density profile from beam and halo H α emission data (BES, colored squares + line) for a series of time points each 600 ms apart. The shown Thomson data points (TS, black dots) are normalized using the interferometer data. Right: the simultaneously inferred beam power and power component fractions for each time point. The squares are indicating the values inferred from the BES data. The plotted lines show the nominal values from other diagnostics. The fraction of beam power injected in form of particles with energy E , $\frac{E}{2}$ or $\frac{E}{3}$ is denoted p_1 , p_2 and p_3 .

MAP inferred profiles. The inference is very stable over time, yielding the same profiles at different time points in the outer half of the plasma. The Thomson data and the BES inferred profiles agree on the position in the plasma where the strongest gradients can be seen ($\rho \approx 0.4$). The magnitude of the peaking agrees very well with the interferometer scaled Thomson profiles for the last two time points. For the first two time points a 10% higher core density is inferred from the BES data than seen in the Thomson data. This still lies within the estimated uncertainties of both systems. At each time step the total into the plasma injected beam power as well as the power component fractions were free parameters during the inversion. In the bottom plot of figure 5 the inferred parameters (squares) are compared to the nominal values (drawn as lines) supplied by other diagnostics. The total beam power is drawn in black and the fractions in different colors. The nominal values stay almost constant over the course of the discharge. The inferred values from the BES data not only agree with the nominal values but as well show only little variation over time. Inferring the same beam parameters at different phases of the discharge with strongly differing density profiles underlines the consistency of the model and the data.

Recalling from figure 3 that the beam and halo emission can mostly be separated in the measured spectra and that both depend on the electron density, it is interesting to study if the density profile can be inferred from the beam or halo emission exclusively. To infer the profile only from the beam emission the central wavelength interval containing the halo emission is cut from the spectra before the fitting process. Contrary, when only using the halo emission all measured data at smaller or higher wavelengths than the halo emission is cut from the spectra before fitting.

In figure 6 the results are shown for two discharges. The reference lines are the fitted profiles using the full spectrum (red line + stars) which were already shown in figure 4. It can be seen that the density profile can also be inferred exclusively from beam (blue dotted line) or halo (blue dashed dotted line) emission. They both agree in shape and magnitude with the profiles fitted from the full spectra. It has to be emphasized that the only free parameters in these fits were the density profile, the total beam power and the beam component fractions. The necessary inference of the alignment of the optical heads and beams, the beam power and the beam shape was performed on multiple discharges in the same campaign where the full spectra were used. After fitting and fixing these parameters, inferring the density profile from just the beam emission part of the spectra speeds up the inference significantly as the forward model does not need to solve the halo CX diffusion equation. A profile for a single time point can then be computed on six CPU cores in about 2 min instead of 20 min. It is currently under investigation if it is possible to get an estimate of the core electron density from just a few core channels by comparing beam and halo emission between these. This could again reduce the computation time by an order of magnitude.

3.2. Main ion temperature profile inference

There is only little information on the main ion temperature profile contained in the beam emission part of the spectra as the light emitted by excited neutral beam particles is not thermally Doppler broadened. The intensity of the beam emission at any point in the plasma is dominantly determined by the beam and plasma density and the emission rate coefficient is not strongly affected by the ion temperature as the beam particles are a

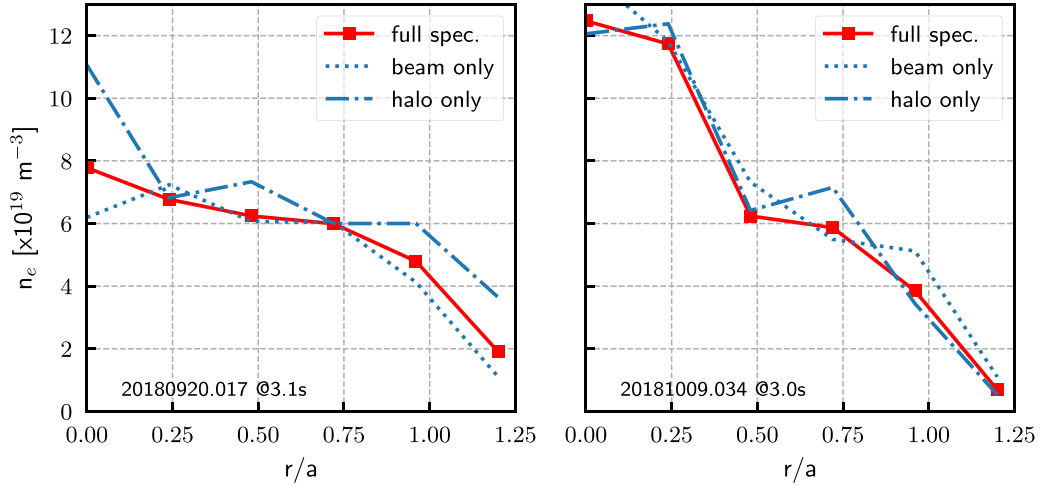


Figure 6. Inference of the electron density profile using only a part of the $H\alpha$ spectra. The profile inferred from beam (halo) emission only is shown as a dotted blue line (dotted dashed blue line). The profile inferred from the full spectra is shown in red as a reference.

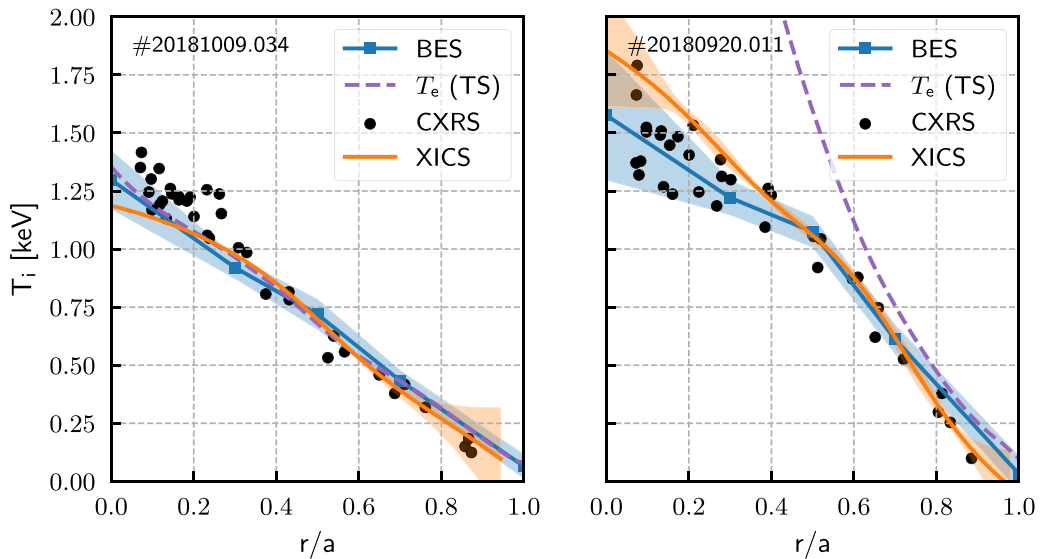


Figure 7. Main ion and electron radial temperature profiles in a single beam discharge. The inferred ion temperature profile (blue line + stars) from beam and halo $H\alpha$ emission is compared to data from the charge exchange recombination system (black dots) system measuring carbon emission and a fit of x-ray imaging crystal spectrometer (XICS) data (orange line) corrected by subtracting 200 eV. The electron temperature profile (purple dashed line) is a lowest fit of data from the Thomson scattering system.

factor of $\approx 8/5/4$ (corresponding to the three injection energies) faster than the average plasma ion at a temperature of 1 keV. The halo, on the other hand, consists of CX neutrals which have the same temperature as the surrounding plasma. Consequently, the halo emission at a point in the plasma is Doppler broadened proportionally to the local main ion temperature. The total halo emission along a line of sight is a function of the integrated halo density distribution at different temperatures. The shape of the halo cloud surrounding the beam is determined by CX diffusion processes which are in itself dependent on the ion temperature profile. All of these effects are included in the implemented forward model.

In figure 7 the inferred ion temperature profiles (blue lines + stars) are shown for two discharges (#20181009.034, #20180920.011) which were already described and used to

fit density profiles in the previous section. The fitted profiles are compared to data from the CXRS system [21] (black dots) measuring carbon emission and a fit of x-ray imaging crystal spectrometer (XICS) data [16, 23] (orange line). The XICS data is corrected by subtracting 200 eV at every radial point. It is assumed that the carbon impurity ion temperature is the same as the plasma ion temperature as the collision cross sections between impurity ions and plasma ions (protons in these cases) are much larger than between those impurities and any hotter species (electrons in ECR heated plasmas and/or fast-ions in NBI plasmas). It was also verified that the argon and carbon impurity ion temperatures measured with the CXRS system are the same, which indicates that the different ion species are in equilibrium. The fast ion content in the presented discharges is too small to cause

significant deviations from a Maxwellian distribution of the plasma ions. CX of the beam and recycling neutrals with fast ions in the plasma produce a contribution to the H-alpha spectrum. However, the signal is at least two orders of magnitude smaller than the main ion halo feature [24] and does not significantly bias the density or temperature determined from the halo component.

A local regression fit of the Thomson data for the electron temperature is shown in purple (dashed line). In the ECR heated discharge (#20180920.011), plotted on the right side, all three T_i diagnostics agree very well around mid radius from $r/a = 0.3$ to 0.7 . The XICS system measures a higher ion temperature in the plasma core at radii $\rho < 0.2$ than the CXRS system or the BES system, however, the uncertainty of the XICS value increases in the core and at the very edge. Except for two outliers the CXRS system seems to agree with the inferred profile in the plasma core. At the plasma edge ($r/a > 0.8$) the BES inferred profile is almost equal to the electron temperature measured by the Thomson system. In the purely NBI heated discharge (#20181009.034) the ion temperature profiles of the three independent diagnostics agree very well. Only in the plasma core at $r/a < 0.2$ the XICS system measures a $\approx 10\%$ lower temperature. At radii further to the plasma edge the ion and electron temperature are expected to equalize due to the high collisionality and the large plasma volume. As expected, the inferred ion temperature and the electron temperature are almost equal at radii $\rho > 0.7$ in both discharges.

4. Conclusion

In the presented analysis the Bayesian inference framework Minerva was used to infer electron density profiles and ion temperature profiles from neutral beam (hydrogen) and halo Balmer- α emission data.

It has been shown that the Balmer- α spectra contain sufficient information to independently reconstruct complete profiles of both the electron density and ion temperature that compare well with other diagnostics. Since this information is non-trivially contained in a combination of the BES and halo intensities as well as the beam attenuation, a complete and detailed forward model is required to access it.

As the exact shape and magnitude of the measured Balmer- α spectra depend on the beam parameters (power, species fractions, divergence) and the alignment of the optical head, fitting plasma profiles from the data of the multiple lines of sight is not straight forward. The Minerva software framework, specifically designed for forward modeling and inference, significantly eased the implementation of this complex problem. The Bayesian ansatz of this framework also allows the uncertainties of the total beam power and neutral beam fractions to be included consistently.

The density and ion temperature profile inference was successfully performed on a range of plasmas with differing conditions regarding heating and absolute plasma density. The time evolution of the electron density profile in a non steady-state discharge was captured well. It could be shown that even from a subset of the data, including only the halo or

beam emission part of the spectra respectively, the full electron density profile could be inferred. Having only to evaluate the beam part of the forward model speeds up the inference significantly.

As the whole optical system is absolutely calibrated the inferred profiles do not only fit the shape but also the magnitude of the real profile. No rescaling using interferometer data was performed as is usually done for the Thomson electron density data at W7-X. Thereby the fitted profiles represent a fully independent measurement.









Data availability statement

The data cannot be made publicly available upon publication because they are owned by a third party and the terms of use prevent public distribution. The data that support the findings of this study are available upon reasonable request from the authors.

Acknowledgment

This work has been carried out within the framework of the EUROfusion Consortium, funded by the European Union via the Euratom Research and Training Programme (Grant Agreement No 101052200—EUROfusion). Views and opinions expressed are however those of the author(s) only and do not necessarily reflect those of the European Union or the European Commission. Neither the European Union nor the European Commission can be held responsible for them.

ORCID iDs

S Bannmann  <https://orcid.org/0000-0003-0772-9278>
 P Zs Poloskei  <https://orcid.org/0000-0001-7781-5599>
 A Pavone  <https://orcid.org/0000-0003-2398-966X>
 S Kwak  <https://orcid.org/0000-0001-7874-7575>
 S Lazerson  <https://orcid.org/0000-0001-8002-0121>
 D Hartmann  <https://orcid.org/0000-0002-3511-6500>
 A Langenberg  <https://orcid.org/0000-0002-2107-5488>
 K J Brunner  <https://orcid.org/0000-0002-0974-0457>
 R C Wolf  <https://orcid.org/0000-0002-2606-5289>

References

- [1] Wolf R C, Beidler C D, Dinklage A, Helander P, Laqua H P, Schauer F, Sunn P T and Warmer F 2016 Wendelstein 7-X program-demonstration of a stellarator option for fusion energy *IEEE Trans. Plasma Sci.* **44** 1466–71
- [2] Wolf R *et al* 2017 Major results from the first plasma campaign of the Wendelstein 7-X stellarator *Nucl. Fusion* **57** 102020
- [3] Beidler C D *et al* 2021 Demonstration of reduced neoclassical energy transport in Wendelstein 7-X *Nature* **596** 221–6
- [4] Pasch E, Beurskens M N A, Bozhnikov S A, Fuchert G, Knauer J and Wolf R C (Team W X) 2016 The Thomson scattering system at Wendelstein 7-X *Rev. Sci. Instrum.* **87** 11E729
- [5] Bozhnikov S *et al* 2017 The Thomson scattering diagnostic at Wendelstein 7-X and its performance in the first operation phase *J. Instrum.* **12** 10004

- [6] Brunner K, Akiyama T, Hirsch M, Knauer J, Kornejew P, Kursinski B, Laqua H, Meineke J, Mora H T and Wolf R C 2018 Real-time dispersion interferometry for density feedback in fusion devices *J. Instrum.* **13** 09002
- [7] Mandl W, Wolf R C, von Hellermann M G and Summers H P 1993 Beam emission spectroscopy as a comprehensive plasma diagnostic tool *Plasma Phys. Control. Fusion* **35** 1373–94
- [8] Bannmann S *et al* 2023 Fast forward modeling of neutral beam injection and halo formation including full Balmer- α emission prediction at W7-X *J. Instrum.* **18** 10029
- [9] Levinton F M 1999 The motional Stark effect: overview and future development (invited) *Rev. Sci. Instrum.* **70** 810–4
- [10] Svensson J and Werner A 2007 Large scale Bayesian data analysis for nuclear fusion experiments *IEEE Int. Symp. on Intelligent Signal Processing* pp 1–6
- [11] Kwak S, Svensson J, Brix M and Ghim Y (JET Contributors) 2017 Bayesian electron density inference from JET lithium beam emission spectra using Gaussian processes *Nucl. Fusion* **57** 036017
- [12] Schmitz O *et al* 2008 Status of electron temperature and density measurement with beam emission spectroscopy on thermal helium at textor *Plasma Phys. Control. Fusion* **50** 115004
- [13] Barbui T *et al* 2020 Measurements of plasma parameters in the divertor island of Wendelstein 7-X through line-ratio spectroscopy on helium *Nucl. Fusion* **60** 106014
- [14] Flom E *et al* 2022 Bayesian modeling of collisional-radiative models applicable to thermal helium beam plasma diagnostics *Nucl. Mater. Energy* **33** 101269
- [15] Svensson J, von Hellermann M and König R W T 2001 Direct measurement of JET local deuteron densities by neural network modelling of Balmer alpha beam emission spectra *Plasma Phys. Control. Fusion* **43** 389
- [16] Langenberg A *et al* 2019 Inference of temperature and density profiles via forward modeling of an x-ray imaging crystal spectrometer within the Minerva Bayesian analysis framework *Rev. Sci. Instrum.* **90** 063505
- [17] Haskey S R *et al* 2018 Active spectroscopy measurements of the deuterium temperature, rotation and density from the core to scrape off layer on the DIII-D tokamak (invited) *Rev. Sci. Instrum.* **89** 10D110
- [18] Salewski M *et al* 2018 Deuterium temperature, drift velocity and density measurements in non-Maxwellian plasmas at ASDEX Upgrade *Nucl. Fusion* **58** 036017
- [19] Lazerson S A *et al* 2021 First neutral beam experiments on Wendelstein 7-X *Nucl. Fusion* **61** 096008
- [20] McNeely P *et al* 2013 Current status of the neutral beam heating system of W7-X *Fusion Eng. Des.* **88** 1034–7
- [21] Ford O P *et al* 2020 Charge exchange recombination spectroscopy at Wendelstein 7-X *Rev. Sci. Instrum.* **91** 023507
- [22] Pavone A *et al* 2019 Measurements of visible Bremsstrahlung and automatic Bayesian inference of the effective plasma charge z_{eff} at W7-X *J. Instrum.* **14** C10003
- [23] Kring J, Pablant N, Langenberg A, Rice J, Delgado-Aparicio L, Maurer D, Traverso P, Bitter M, Hill K and Reinke M 2018 *In situ* wavelength calibration system for the x-ray imaging crystal spectrometer (XICS) on W7-X *Rev. Sci. Instrum.* **89** 10F107
- [24] Poloskei P Z, Geiger B, van Vuuren A J, Äkäslompolo S, Ford O, Spanier A, Neelis T, McNeely P and Hartmann D (the W7-X Team) 2023 Experimental characterization of the active and passive fast-ion H-alpha emission in W7-X using FIDASIM *Nucl. Fusion* **64** 026008